# Microelectromechanical Systems Cantilever Resonators Under Soft Alternating Current Voltage of Frequency Near Natural Frequency

**Dumitru I. Caruntu**[1]
Mem. ASME
Mechanical Engineering Department,
University of Texas Pan American,
1201 W University Drive,
Edinburg, TX 78539
e-mail: caruntud@utpa.edu

**Martin W. Knecht**
Engineering Department,
South Texas College,
McAllen, TX 78501
e-mail: mknecht@southtexascollege.edu

*This paper deals with nonlinear-parametric frequency response of alternating current (AC) near natural frequency electrostatically actuated microelectromechanical systems (MEMS) cantilever resonators. The model includes fringe and Casimir effects, and damping. Method of multiple scales (MMS) and reduced order model (ROM) method are used to investigate the case of weak nonlinearities. It is reported for uniform resonators: (1) an excellent agreement between the two methods for amplitudes less than half of the gap, (2) a significant influence of fringe effect and damping on bifurcation frequencies and phase–frequency response, respectively, (3) an increase of nonzero amplitudes' frequency range with voltage increase and damping decrease, and (4) a negligible Casimir effect at microscale*. [DOI: 10.1115/1.4028887]

## Introduction

Microelectromechanicals systems (MEMS) find their use in biomedical, automotive, and aerospace. MEMS beams are common and successfully used as chemical sensors [1], biosensors [2], pressure sensors [3], switches [4], and energy harvesters [5]. MEMS systems are nonlinear due to actuation forces, damping effects, large structural deformation, and intermolecular surface forces, such as Casimir and/or van der Waals, which are significant for gaps less than 200 nm [6]. Structural nonlinearities are significant for short beams and/or large deflections. Nonlinearities due to damping effects, such as squeeze film damping, can be neglected within certain pressure regimes [7,8] or when considering steady state behavior [9]. Conversely nonlinearities from electrostatic forces cannot be neglected [10].

Parametrically excited MEMS resonators via electrostatic actuation are highly dependent on parameters [9,11–13]. MEMS cantilevers with periodic coefficients in both linear and nonlinear terms of the equation of motion [11] have been reported. Clamped–clamped resonators using the method of multiple scales (MMS) and reduced order model (ROM) method have been investigated [14]. Yet, fringe correction and Casimir effect have not been considered, and the second harmonic has been neglected due to the direct current (DC) voltage much larger than the AC voltage in Ref. [14]. Electrostatically actuated MEMS resonators modeled as mass–spring–damper system have been investigated using the method of averaging [9] and their frequency response and stability found. Yet, it lacked numerical validation, continuous system modeling, and fringe correction effect. Frequency response of cantilever resonators has been reported [15–21]. Forces driving the resonator in these investigations were due to thermal (Brownian) excitation and fluid hydrodynamics. Yet, such forces did not produce parametric excitations or nonlinear behavior. Parametric resonance of a MEMS cantilever [22] has been created via a feedback scheme on a piezoelectrically driven microcantilever using a linear Mathieu's equation as the governing equation of motion. Yet, the parametric coefficient was only in the linear terms. Nonlinear behavior of electrostatically actuated cantilever beam micro resonators, including fringe effect, has been investigated [11] using MMS and ROM. Yet, the nonlinear behavior was due to AC voltage of frequency near a system's half natural frequency of the resonator, which resulted in primary resonance. However, resonances occur at various excitation frequencies due to the parametric excitation [11–13,23].

Partial differential equations of motion of such MEMS continuous systems can be solved using analytical methods such as averaging, harmonic balance, or MMS [11,24], and numerical methods such as finite element (FEM), boundary-element (BEM), finite difference (FDM), and ROM method [24]. FEM, BEM, and FDM methods are relatively accurate. Yet, they are only adequate for static systems, which require less computational time and cost than dynamic systems.

In this paper, the nonlinear parametric behavior of MEMS cantilever resonators due to AC of frequency near a system's natural frequency electrostatic actuation is investigated. This leads to parametric resonance as shown afterwards. An Euler–Bernoulli MEMS cantilever including electrostatic force, fringe effect, damping, and Casimir effect is investigated using MMS and ROM [11,24–26]. MMS is applied directly to the dimensionless partial differential equation of motion of the system in order to obtain analytically the amplitude–frequency response. It is showed that at micro scale the Casimir effect is negligible.

To the best of our knowledge, this is for the first time when for electrostatically actuated MEMS cantilever resonators: (1) parametric resonance due to only soft AC voltage leading to a soft force of two components, constant and second harmonic [11], is considered. Soft actuation can be used for microbalances due to very small power consumption. (2) An approach in which the model includes periodic coefficients in the nonlinear terms is considered. The model includes linear parametric, nonlinear, and most importantly parametric-nonlinear terms. This is in contrast with other works on parametrically excited beams. For instance, AC voltage was much smaller than the DC voltage in Ref. [27], which led to very small nonlinear parametric terms that were neglected in the MMS. (3) The convergence of ROM frequency response using two, three, four, and five terms is reported as well. (4) A direct comparison between MMS and ROM is reported.

[1]University of Texas Pan American becomes University of Texas Rio Grande Valley starting Fall 2015, e-mail: caruntud2@asme.org; dcaruntu@yahoo.com.

Contributed by the Dynamic Systems Division of ASME for publication in the Journal of Dynamic Systems, Measurement, and Control. Manuscript received November 6, 2012; final manuscript received August 16, 2014; published online January 9, 2015. Assoc. Editor: Qingze Zou.

This work shows that: (1) the approach in which the MMS model includes the periodic coefficients in the nonlinear gives an excellent agreement between MMS and ROM of any number of terms for amplitudes less than 0.5 of the gap. (2) The pull-in from large amplitudes is predicted only by four or more terms in the ROM, (3) while two and three terms ROM and MMS fail in this prediction. (4) Casimir effect is negligible at microscale. This effect is a point of future investigation at nanoscale levels. Also, (5) the influences of damping, voltage, and fringe effect on the frequency response of the MEMS cantilever resonator are reported.

## Equation of Motion

Electrostatically actuated system to be investigated consists of a conducting elastic MEMS cantilever over a rigid stationary conducting plate (ground plate) (Fig. 1). Between the beam and plate is a dielectric fluid such as air. Motion equation is based on Euler–Bernoulli theory (structural nonlinearities are neglected) and includes electrostatic, viscous damping, and nanoscale surface forces such as Casimir. The electrostatic force includes a first-order fringe field correction based on Palmer's formula [10]. The electrostatic force is produced by applying a potential difference between the flexible MEMS cantilever and the rigid plate, Fig. 1, $V(t) = V_p + V_0\cos(\Omega t)$, where $V_p$ is the polarizing DC voltage, and $V_0$ and $\Omega$ are the AC voltage and excitation frequency. Since the electrostatic force is proportional to the square of the voltage, there are three components: constant $V_p^2 + 0.5V_0^2$, first harmonic $2V_pV_0\cos(\Omega t)$, and second harmonic $0.5V_0^2\cos(2\Omega t)$ [11]. In this work, $V_p = 0$, therefore, only the second harmonic is present

$$V(t)^2 = \frac{V_0^2}{2} + \frac{V_0^2}{2}\cos(2\Omega t) \tag{1}$$

However, $V_0$ contributes to a static voltage, despite the lack of a DC voltage. Therefore, the resonator vibrates about a deformed position (not the position at rest). All forces in the system, except damping, are nonlinear. In this work the case of uniform MEMS cantilever resonators. The boundary value problem of electrostatically actuated uniform MEMS cantilevers [11,25,26] is given by

$$\begin{cases} \dfrac{\partial^2 u}{\partial \tau^2} + \dfrac{\partial^4 u}{\partial z^4} = -b^*\dfrac{\partial u}{\partial \tau} + \dfrac{\alpha}{(1-u)^4} + \dfrac{\delta}{(1-u)^2}V^2(\tau) \\ \qquad\qquad + f\dfrac{\delta}{(1-u)}V^2(\tau) \\ u(0) = \dfrac{\partial u}{\partial z}(0) = \dfrac{\partial^2 u}{\partial z^2}(1) = \dfrac{\partial^3 u}{\partial z^3}(1) = 0 \end{cases} \tag{2}$$

where $V(\tau)$ is the dimensionless voltage, and $u$, $z$, and $\tau$ are beam dimensionless deflection, dimensionless longitudinal coordinate, and dimensionless time, respectively

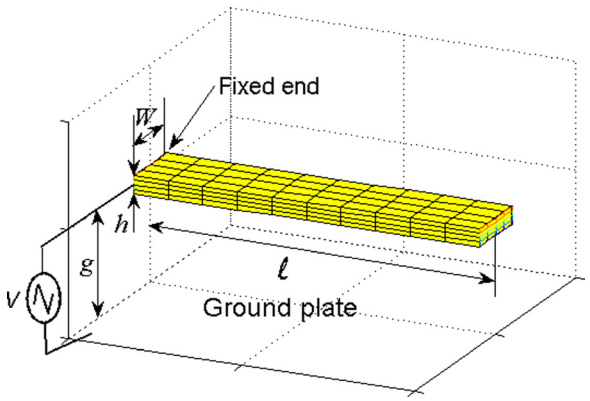


**Fig. 1 Uniform MEMS cantilever resonator**

$$u = w/g, \quad z = x/\ell, \quad \tau = \frac{1}{\ell^2}\sqrt{\frac{EI_0}{\rho A_0}}\cdot t \tag{3}$$

Constant $\rho$ is the beam density, $A_0$ is the cross-sectional area, $w$ is the dimensional beam deflection, $t$ is the dimensional time, $E$ is the Young modulus, $I_0$ is the cross-sectional moment of inertia, $x$ is the dimensional longitudinal coordinate, $\ell$ is the cantilever length, and $g$ is the gap (Fig. 1). The dimensionless parameters of Eq. (2), Casimir effect $\alpha$, electrostatic excitation (voltage) $\delta$, fringe effect $f$, damping $b^*$, and dimensionless frequency $\omega^*$, are [11,25,26] given by

$$\begin{gathered} \alpha = \frac{\pi^2\hbar c W\ell^4}{240g^5EI_0}, \quad \delta = \frac{\varepsilon_0 W\ell^4}{2g^3EI_0}V_0^2, \quad f = \frac{0.65g}{W}, \\ b^* = b\sqrt{\frac{\ell^4}{\rho A_0 EI_0}}, \quad \omega^* = \omega\ell^2\sqrt{\frac{\rho A_0}{EI_0}} \end{gathered} \tag{4}$$

where $\hbar = 1.055\times10^{-34}$ J s is Planck's constant divided by $2\pi$, $c = 2.998\times10^8$ m s$^{-1}$ is the speed of light, $\varepsilon_0 = 8.854\times10^{-12}$ C$^2$ N$^{-1}$ m$^{-2}$ is the permittivity of free space, $W$ is the beam width, $b$ is the damping coefficient, and $V_0$ is the amplitude of the AC voltage. From this point forward, dimensionless natural frequencies of the MEMS cantilever are denoted simply by $\omega_k$.

## AC Near Natural Frequency $\Omega^* \approx \omega_k$, Parametric Resonance

The dimensionless AC voltage considered in this investigation is given by

$$V(\tau) = \cos\Omega^* T_0, \quad \Omega^* = \Omega\ell^2\sqrt{\frac{\rho A_0}{EI_0}} \tag{5}$$

where $\Omega^*$ and $\Omega$ are the dimensionless frequency of excitation and its corresponding dimensional frequency, respectively. $V^2(\tau)$ in terms of imaginary exponentials is

$$V^2(T_0) = \frac{1}{2} + \frac{1}{4}\left(e^{2\Omega^* iT_0} + e^{-2\Omega^* iT_0}\right) \tag{6}$$

AC near natural frequency $\Omega^* \approx \omega_k$ can be written as

$$\Omega^* = \omega_k + \varepsilon\sigma \tag{7}$$

where $\omega_k$ is dimensionless natural frequency of the MEMS cantilever resonator, $\sigma$ is a detuning parameter, and $\varepsilon$ is a small book-keeping device. The resulting resonance is a subharmonic resonance, namely, parametric resonance, since the electrostatic force (to include fringe effect) is near twice natural frequency Eqs. (2), (6), and (7).

## Method of Multiple Scales (MMS)

The frequency response of the resonator is investigated using MMS [11,25,26], a perturbation method valid for weak nonlinearities and small to moderate amplitudes. Therefore, soft nonlinear parametric actuation, soft Casimir effect, soft damping, and small to moderate deflections are considered, i.e., the parameters given by Eq. (4) are small. MMS and ROM results are compared in a later section, namely Numerical Solutions for Uniform MEMS Resonators.

**Direct Approach of the Problem.** Expanding in Taylor series the right-hand side terms of Eq. (2) up to third-order in $u$ around $u = 0$, Eq. (2) for small parameters $\alpha, \delta, f$, and $b^*$ can be written as

$$\begin{aligned} \frac{\partial^2 u}{\partial \tau^2} + \frac{\partial^4 u}{\partial z^4} = &-\varepsilon b^*\frac{\partial u}{\partial \tau} + \varepsilon\alpha[1 + 4u + 10u^2 + 20u^3] \\ &+ \varepsilon\delta[(1+f) + (2+f)u + (3+f)u^2 \\ &+ (4+f)u^3]V^2(\tau) \end{aligned} \tag{8}$$

where $\varepsilon$ is a small dimensionless bookkeeping parameter. MMS is then directly applied to Eq. (8). A first-order expansion of $u$ is considered as follows:

$$u(z,\tau,\varepsilon) = u_0(z,T_0,T_1) + \varepsilon \cdot u_1(z,T_0,T_1) \tag{9}$$

where $T_0 = \tau$ is fast time scale and $T_1 = \varepsilon \cdot \tau$ is slow time scale. The time derivative becomes $\partial/\partial\tau = D_0 + \varepsilon \cdot D_1$, where $D_n = \partial/\partial T_n$, $n = 0,1$. Replacing Eq. (9) and time derivatives into Eq. (8), and collecting coefficients of like powers of $\varepsilon$, two approximation problems, zero-order and first-order, respectively, result as

$$\text{Order } \varepsilon^0 \begin{cases} D_0^2 u_0 + \dfrac{\partial^4 u_0}{\partial z^4} = 0 \\ u_0(0) = \dfrac{\partial u_0}{\partial z}(0) = \dfrac{\partial^2 u_0}{\partial z^2}(1) = \dfrac{\partial^3 u_0}{\partial z^3}(1) = 0 \end{cases} \tag{10}$$

$$\text{Order } \varepsilon^1 \begin{cases} D_0^2 u_1 + \dfrac{\partial^4 u_1}{\partial z^4} = -2D_0 D_1 u_0 - b^* D_0 u_0 \\ \qquad + \alpha[1 + 4u_0 + 10u_0^2 + 20u_0^3] \\ \qquad + \delta[(1+f) + (2+f)u_0 + (3+f)u_0^2 \\ \qquad + (4+f)u_0^3]V^2(T_0) \\ u_1(0) = \dfrac{\partial u_1}{\partial z}(0) = \dfrac{\partial^2 u_1}{\partial z^2}(1) = \dfrac{\partial^3 u_1}{\partial z^3}(1) = 0 \end{cases} \tag{11}$$

**Zero-Order Approximation.** The solution $u_0$ of Eq. (10) is given by [11,25,26]

$$u_0(z,T_0,T_1) = \varphi(z)\left[A(T_1)e^{i\omega T_0} + \overline{A}(T_1)e^{-i\omega T_0}\right] \tag{12}$$

where $A$ and $\overline{A}$ are complex conjugate coefficients to be determined. Equation (12) must satisfy the boundary conditions of Eq. (10). This gives the natural frequencies $\omega_k$ and the mode shapes $\varphi_k(z)$ of the MEMS cantilever. Natural modes for uniform cantilevers and cantilevers of varying thickness [28,29], and examples of using factorization method [30,31] are reported in the literature. The mode shapes $\varphi_k(z)$ [11,25,26,28] form an orthonormal set. They satisfy

$$\begin{cases} \varphi_k^{(4)} = \omega_k^2 \varphi_k \\ \varphi_k(0) = \varphi_k'(0) = \varphi_k''(1) = \varphi_k'''(1) = 0 \end{cases}, \quad \langle \varphi_m, \varphi_n \rangle = \int_0^1 \varphi_m \varphi_n dz = \delta_{mn} \tag{13}$$

where $\delta_{mn}$ is Kronecker's delta.

**First-Order Approximation.** The first-order approximation might be found by solving the inhomogeneous Eq. (11). Replacing Eq. (12) for the $k$th mode into Eq. (11), it results

$$\begin{aligned} D_0^2 u_1 + \frac{\partial^4 u_1}{\partial z^4} = & -2D_0 D_1 \varphi_k \left[A_k(T_1)e^{i\omega_k T_0} + \overline{A_k}(T_1)e^{-i\omega_k T_0}\right] \\ & - b^* D_0 \varphi_k \left[A_k(T_1)e^{i\omega_k T_0} + \overline{A_k}(T_1)e^{-i\omega_k T_0}\right] \\ & + \alpha\Big\{1 + 4\varphi_k\left[A_k(T_1)e^{i\omega_k T_0} + \overline{A_k}(T_1)e^{-i\omega_k T_0}\right] \\ & + 10\varphi_k^2\left[A_k(T_1)e^{i\omega_k T_0} + \overline{A_k}(T_1)e^{-i\omega_k T_0}\right] \\ & + 20\varphi_k^2\left[A_k(T_1)e^{i\omega_k T_0} + \overline{A_k}(T_1)e^{-i\omega_k T_0}\right]^3\Big\} \\ & + \delta\Big\{(1+f) + (2+f)\varphi_k\left[A_k(T_1)e^{i\omega_k T_0}\right. \\ & \left. + \overline{A_k}(T_1)e^{-i\omega_k T_0}\right] + (3+f)\varphi_k^2 \\ & \times \left[A_k(T_1)e^{i\omega_k T_0} + \overline{A_k}(T_1)e^{-i\omega_k T_0}\right]^2 \\ & + (4+f)\varphi_k^3\left[A_k(T_1)e^{i\omega_k T_0}\right. \\ & \left. + \overline{A_k}(T_1)e^{-i\omega_k T_0}\right]^3\Big\} \cdot V^2(T_0) \end{aligned} \tag{14}$$

Substitute Eqs. (6) and (7) into Eq. (14). A solvability condition requires that the right-hand side of Eq. (14) is orthogonal to every solution of the homogenous problem Eq. (10). Applying the orthogonality condition, multiplying by $\varphi_k(z)$ and integrating from 0 to 1, collecting all secular terms and set the sum equal to zero, one obtains

$$\begin{aligned} & -2i\omega_k g_{1kk} A_k' - i\omega_k b^* g_{1kk} A_k + [4\alpha + C_2] g_{1kk} A_k \\ & + 3[20\alpha + C_4] g_{3kk} A_k^2 \bar{A}_k + \frac{1}{2} C_2 g_{1kk} \bar{A}_k e^{2i\sigma T_1} \\ & + \frac{3}{2} C_4 g_{3kk} A_k \bar{A}_k^2 e^{2i\sigma T_1} + \frac{1}{2} C_4 g_{3kk} A_k^3 e^{-2i\sigma T_1} = 0 \end{aligned} \tag{15}$$

where

$$C_m = \frac{1}{2}(m+f)\delta, \quad m = 1,2,3,4, \quad g_{nkk} = \langle \varphi_k^n, \varphi_k \rangle = \int_0^1 \varphi_k^n \varphi_k dz \tag{16}$$

$A_k'$ is the derivative of $A_k$ with respect to the slow time scale $T_1$, and $n$ is positive integer. Express $A_k$ in polar form

$$A_k = \frac{1}{2} a_k e^{i\beta_k} \tag{17}$$

where $a_k$ and $\beta_k$ are real and represent the amplitude of the resonator's motion and its phase relative to excitation, respectively. Substituting Eq. (17) into Eq. (15) and separating the real and imaginary parts, the amplitude–phase differential equations result as follows:

$$a_k' = a_k\left\{-\frac{b^*}{2} + \left[C_2 + \frac{C_4}{2}\frac{g_{3kk}}{g_{1kk}}a_k^2\right]\frac{\sin 2\gamma_k}{4\omega_k}\right\} \tag{18}$$

$$\begin{aligned} a_k\gamma_k' = & a_k\sigma + \frac{(4\alpha + C_2)}{2\omega_k}a_k + \frac{3(20\alpha + C_4)}{8\omega_k}\frac{g_{3kk}}{g_{1kk}}a_k^3 \\ & + a_k\left[C_2 + C_4\frac{g_{3kk}}{g_{1kk}}a_k^2\right]\frac{\cos 2\gamma_k}{4\omega_k} \end{aligned} \tag{19}$$

where

$$\gamma_k = \sigma T_1 - \beta_k \tag{20}$$

**Steady-State Solutions.** The steady-state solutions result from substituting $a_k' = \gamma_k' = 0$ into Eqs. (18) and (19). Zero-amplitude steady-state $a_k = 0$ is solution for all values of the detuning parameter $\sigma$. The nonzero amplitude steady-state solutions, the amplitude–frequency response, are as follows:

$$a_k^2 = \frac{2g_{1kk}}{C_4 g_{3kk}}\left(\frac{2\omega_k b^*}{\sin 2\gamma_k} - C_2\right) \tag{21}$$

$$\sigma = -\frac{4\alpha + C_2}{2\omega_k} - \frac{3(20\alpha + C_4)}{8\omega_k}\frac{g_{3kk}}{g_{1kk}}a_k^2 - \left[C_2 + C_4\frac{g_{3kk}}{g_{1kk}}a_k^2\right]\frac{\cos 2\gamma_k}{4\omega_k} \tag{22}$$

Steady-state solutions for uniform MEMS cantilever are showed (graphed) in a later section, namely Numerical Solutions for Uniform MEMS Resonators.

## Reduced Order Model (ROM) Method

It is showed afterward that the Casimir effect is negligible for MEMS resonators ($\alpha = 0$, Tables 1 and 2) in the case of uniform resonators. Therefore, the model is solved using ROM with $\alpha = 0$. For a given frequency and initial amplitude, the time response of the system is found, and consequently the steady-state amplitude for the considered frequency is obtained. Several such steady-state points (amplitude–frequency) are to be determined and

**Table 1 Physical characteristics of a typical microbeam**

| Parameter | Symbol | Value |
|---|---|---|
| Beam width | $W$ | 20 $\mu$m |
| Beam length | $\ell$ | 300 $\mu$m |
| Beam thickness | $h$ | 2.0 $\mu$m |
| Initial gap distance | $g$ | 8.0 $\mu$m |
| Material density | $\rho$ | 2330 kg/m$^3$ |
| Young's modulus | $E$ | 169 GPa |
| Quality factor | $Q$ | 350 |
| Peak AC voltage | $V_0$ | 12.5 V |

**Table 2 Dimensionless parameters**

| Dimensionless parameter | Symbol | Value |
|---|---|---|
| Casimir effect | $\alpha$ | $2.9 \times 10^{-9}$ |
| Amplitude of excitation (voltage) | $\delta$ | 0.10 |
| Fringe correction | $f$ | 0.26 |
| Damping coefficient | $b^*$ | 0.01 |

consequently the frequency–amplitude response of the structure using ROM [11,25,26,32] found. ROM is a Galerkin procedure in which the solution is assumed to be

$$u(z,\tau) = \sum_{k=1}^{N} u_k(\tau)\varphi_k(z) \tag{23}$$

where the number of terms $N$ is finite, $\varphi_k(z)$ are the mode shapes of the MEMS resonator and form a basis of functions, and $u_k(\tau)$ are time dependent functions to be found. The mode shapes in Eq. (23) are reported in the literature [11,25,26,28]. When constructing a ROM, the treatment of the excitation force is very important. Exact form of the forcing function must be used to numerically solve the equations of motion accurately [11,33]. Erroneous results were produced when the forcing function was Taylor expanded up to third power. In addition, the number of terms in Eq. (23) must be at least $N = 3$ for the solutions to converge [11,25,26,33]. To implement this procedure (ROM), Eq. (2) is multiplied by $(1-u)^2$ to eliminate any displacement terms $u$ from appearing in the denominator, and Eqs. (13) and (23) are substituted into the result. Notice that $\alpha = 0$. Multiplying by $\varphi_n(z)$, and integrating the resulting equation from $z = 0$ to 1, the ROM of the system results as follows:

$$\begin{aligned}
&\ddot{u}_n - 2\sum_{i,j=1}^{N} \ddot{u}_i u_j \int_0^1 \varphi_i\varphi_j\varphi_n dz + \sum_{i,j,k=1}^{N} \ddot{u}_i u_j u_k \int_0^1 \varphi_i\varphi_j\varphi_k\varphi_n dz + b^*\dot{u}_n \\
&- 2b^*\sum_{i,j=1}^{N} \dot{u}_i u_j \int_0^1 \varphi_i\varphi_j\varphi_n dz + b^*\sum_{i,j,k=1}^{N} \dot{u}_i u_j u_k \int_0^1 \varphi_i\varphi_j\varphi_k\varphi_n dz \\
&+ \omega_n^2 u_n - 2\sum_{i,j=1}^{N} \omega_i^2 u_i u_j \int_0^1 \varphi_i\varphi_j\varphi_n dz \\
&+ \sum_{i,j,k=1}^{N} \omega_i^2 u_i u_j u_k \int_0^1 \varphi_i\varphi_j\varphi_k\varphi_n dz \\
&= (1+f)\delta V^2(\tau)\int_0^1 \varphi_n dz - f\delta V^2(\tau)u_n
\end{aligned} \tag{24}$$

where $n = 1, 2, \ldots, N$. Equation (24) is a system of $N$ nonexplicit coupled, second-order nonlinear ordinary-differential equations.

## Numerical Solutions for Uniform MEMS Resonators

Steady-state analytical solutions by MMS, Eqs. (21) and (22), give the amplitude–frequency and phase–frequency responses. ROM is used to: (1) investigate the time response of the system and test the results obtained using MMS at small amplitudes and (2) predict the behavior of the resonator for larger amplitudes. AC near first natural frequency of MEMS resonator is considered in these numerical simulations.

**Uniform Resonator Characteristics.** Uniform MEMS cantilevers are considered. Their mode shapes, natural frequencies, and coefficients, Eqs. (12,13) are reported in the literature [11,25,26]. Table 1 gives values of the physical characteristics of a typical microbeam [11,25,26]. Dimensionless parameters given by Eq. (4) are given in Table 2. Substituting the values of the dimensionless parameters and $g$ coefficients, given by Eq. (16), into Eqs. (21) and (22), the steady-state frequency–amplitude response for a uniform cantilever is obtained in the case of first mode of vibration.

**Casimir Effect Negligible at MEMS Scale.** The influence of the Casimir force, even though present in the model, does not influence the behavior of the system at the microscale level. Table 2 shows that the Casimir effect parameter $\alpha$ is eight orders of magnitude smaller than the other parameters. For all practical purposes, $\alpha = 0$. Casimir force is significant for gap distances less than one micrometer. Figure 2 shows the change of the dimensionless parameters Eq. (4) as the system is scaled down to nanometer scale. The gap width $g$ is chosen as a scaling factor since the Casimir force depends on it. The other dimensions of the resonator scale proportionally with the gap. Geometric scaling shows that $\alpha$ varies inversely to the gap to the fourth power $g^{-4}$, whereas the electrostatic excitation (voltage) parameter $\delta$ varies inversely to the gap squared $g^{-2}$. Included are the electrostatic force parameters at 0.1 V and 0.5 V. Casimir parameter has same order of magnitude as the electrostatic parameter as the gap distance decreases to 200 nm, which is in agreement with Ref. [6]. If one wants to keep $\delta$ constant while scaling down the resonator, the voltage reduces accordingly (Table 3).

**Steady-State Solutions.** The steady-state solutions given by Eqs. (21) and (22) are parametric equations (parameter $\gamma$). They give the amplitude–frequency and phase–frequency responses for uniform MEMS cantilever resonators, Figures 3(*a*) and 3(*b*), respectively, where $\sigma$ is the detuning dimensionless frequency, Eq. (7) for $\varepsilon = 1$, $U_{\max}$ is the dimensionless amplitude of the tip of the cantilever, $U_{\max} = a \cdot \varphi(1)$, Eqs. (12), (17), and (21), and $\gamma$ is the phase difference between the response and the excitation. For the first mode of vibration, $\varphi(1) = 2$. The steady-state solutions consist of zero-amplitude steady-state solutions (on $\sigma$-axis) and

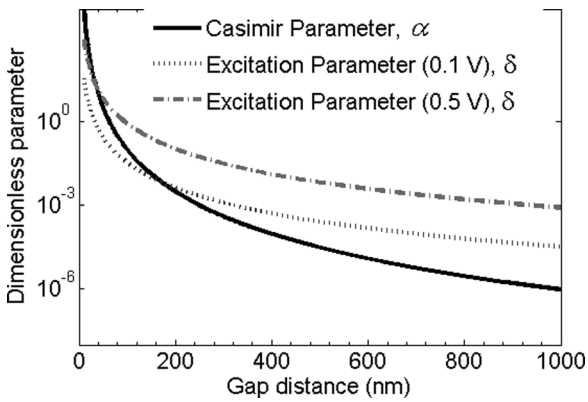


**Fig. 2 Influence of scaling on dimensionless parameters $\alpha$ and $\delta$ with respect to the gap $g$**

**Table 3 Excitation voltages at different scales such that $\delta = 0.1$**

| Geometric scaling factor [g] (m) | Working voltage $V_0$ (V) |
|---|---|
| $10^{-6}$ | 12.5 |
| $10^{-7}$ | 1.2 |
| $10^{-8}$ | 0.12 |

two branches of nonzero-amplitude steady-state solutions, one stable—solid line branch, and the other one unstable—dash branch. To test the stability of steady-state solutions, one uses the Jacobian of Eqs. (21) and (22). For real eigenvalues, one positive and the other negative, the fixed point is a saddle point, which is unstable (the solution diverges) [34], and is located on the dashed line.

The two branches in Fig. 3(*a*) show a softening effect (they are bent to the left, to lower frequencies). The zero-amplitude steady-state solutions exist for all values of frequency detuning parameter $\sigma$. These solutions are unstable between the branches, $-0.0224 = \sigma_B \leq \sigma \leq \sigma_C = -0.0098$, and stable elsewhere. Two distinct Hopf bifurcations, one subcritical (point *B*) and the other one supercritical (point *C*), are shown. The results are similar to those reported for a parametrically excited comb drive [35] and for nonlinearly coupled micromechanical oscillators [36]. The dimensionless amplitude $U_{\max}$ never exceeds unity, i.e., amplitudes cannot be larger than the gap.

Stable solutions are reached as follows. If (1) $\sigma > \sigma_C = -0.0098$, then only zero-amplitude steady-state solutions are reached regardless the initial amplitude, (2) $-0.0224 = \sigma_B \leq \sigma \leq \sigma_C = -0.0098$, then only nonzero stable steady-state amplitudes and/or pull-in phenomenon are reached regardless the initial amplitude, and (3) $\sigma < \sigma_B = -0.0224$, then zero amplitude is reached if the initial amplitude is below the unstable branch, and pull-in phenomenon occurs if the initial amplitude is above the unstable branch. The phase of nonzero amplitudes (Fig. 3(*b*)) is between 1.3 and 1.4 rad. Figure 3(*c*) shows the ROM time response for $\sigma = -0.015$. Resonator tip reaches a steady-state amplitude of $U_{\max} = 0.6$ from initial amplitude $U_0 = 0.01$. A good agreement between the two methods, MMS and ROM, is found for amplitudes less than 0.5 of the gap. ROM, Eq. (24), was transformed into a system of $2N$ first-order differential equations and integrated using MATLAB function *ode15s*.

## Discussion and Conclusions

Nonlinear dynamics of electrostatically actuated MEMS resonators with AC near natural frequency, resulting in parametric resonance, is investigated in this paper. MEMS cantilever is modeled as Euler–Bernoulli beam. The actuation forces are electrostatic, first-order fringe effect, and Casimir. Due to AC voltage, parametric coefficients are found in both linear and nonlinear terms of the governing equation of motion. Nonlinearities arise from electrostatic force and Casimir effect. Casimir effect is negligible at microscale.

Two methods, MMS and ROM, are used in this investigation. "An analytical approach, such as the MMS, allows for a better insight of the dependence of the system on its various parameters, and has the ability to predict interesting phenomena [11]." Approximate analytical techniques require the least amount of computational time and effort, however, at larger amplitudes are the less accurate and cannot predict the behavior of the resonator and pull-in instability as showed afterward [11,25,26]. Despite this, they are very useful in understanding the underlying physics of systems behavior, predicting primary, sub- and super-harmonic resonances, and finding how system's parameters influence its behavior. In this investigation, MMS is directly applied to the partial differential equation of motion in order to find the steady-state solutions. However, MMS is valid only for weak nonlinearities and small to moderate amplitudes. ROM method, a Galerkin procedure, is used to numerically solve the differential equation of motion. ROM is valid for weak and/or strong nonlinearities and small and/or large amplitudes [11,14,25,26,36]. ROM with two, three, four, and five terms are used. The main drawback of ROM method is that resonant zones are not obvious. Using an analytical method such as MMS in conjunction with a numerical method such as ROM allows for identifying the resonance zones and also the behavior of the structure for small and large amplitudes [11]. Another available analytical technique is the method of harmonic balance. We preferred not to use this technique. The downsize of

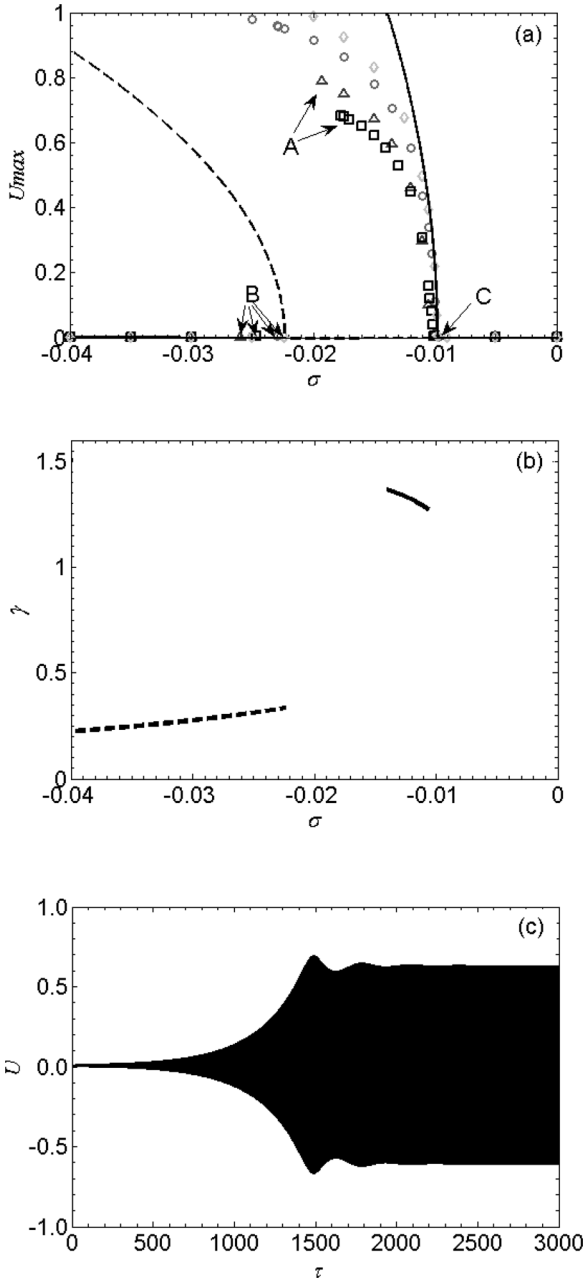


**Fig. 3 Frequency response of the uniform MEMS resonator for AC near first natural frequency using MMS and ROM. The solid and dashed lines are solutions from the MMS representing stable and unstable points, respectively. Parameters values used are $\alpha = 0$, $\delta = 0.1$, $f = 0.26$, and $b^* = 0.01$. (*a*) Amplitude–frequency response using MMS and ROM. The points showed are steady-states using ROM, two terms (diamonds), three terms (circles), four terms (triangles), and five terms (squares). *A* and *B* are points where pull-in is predicted using the four and five term ROMs. *C* is the bifurcation point of the supercritical Hopf bifurcation. (*b*) Phase–frequency response using MMS, and (*c*) time response of the tip of a uniform cantilevered resonator for $\sigma = -0.015$ using the five term ROM method.**

this method is that one needs "to know a great deal about the solution a priori or to carry enough terms in the solution and check the order of the coefficients for all neglected harmonics [37]."

Figure 3(*a*) shows a comparison between the ROM and MMS predictions for frequency–amplitude response. Both methods are in agreement for dimensionless amplitudes less than 0.5. They predict same frequency of the Hopf bifurcation point *C* and a relatively small difference in the frequency of the Hopf bifurcation point *B*, regardless the number of terms in ROM. They also predict the same steady-state stable solutions. For amplitudes larger than 0.5, MMS and ROM solutions are different. This is expected since MMS is valid for small amplitudes. For large amplitudes MMS fails, it overestimates the nonzero stable steady-state amplitudes (branch AC for ROM). Conversely, ROM is able to make accurate predictions including pull-in instability [11,25,26,33] point *A* ($\sigma = -0.018$, $U_{\max} = 0.7$) if five terms are used. The increased accuracy of ROM comes at a cost of increased computational time. If one is only concerned with modeling general system behavior for small to moderate amplitudes, then MMS is suitable. Figure 3(*b*) shows the phase–frequency response. In Fig. 3(*c*), one can see the time response using five terms ROM. Figures 3(*a*) and 3(*c*) are in agreement.

Figure 4 illustrates the effect of damping on the frequency response. As the damping increases, the distance between points *B* and *C* decreases until the stable and unstable branches coalesce in one branch (for $b^* = 0.016$), and then the resulting branch moves to higher amplitudes. The zero amplitude solutions are unstable between points *B* and *C* ($b^* < 0.016$) and stable elsewhere. If $b^* > 0.016$, the zero amplitude steady-state solutions are stable at any frequency since points *B* and *C* do not exist. Nonzero amplitude stable solutions such as those of case $b^* = 0.016$, Fig. 4(*a*), cannot be reached just by frequency sweeps with zero initial amplitude. An external perturbation giving initial amplitudes above the unstable solutions (dashed line) is required to reach nonzero amplitudes or pull-in. For a given frequency in the interval $-0.013 < \sigma < -0.01$, the larger the damping, the lower the nonzero steady-state amplitude (Fig. 4(*a*)). This is in good agreement with Fig. 4(*c*) which shows ROM results for zero initial amplitude $U_0 = 0.0$ and $\sigma = -0.013$. As the damping increases, the time in which steady-state is reached decreases. Figure 4(*b*) shows that damping alters the phase response significantly.

Figure 5 illustrates the effect of the excitation parameter $\delta$ on the frequency response. The excitation factor $\delta$ has a major influence on the amplitude–frequency response (Fig. 5(*a*)). As $\delta$ increases from 0.06 to 0.2: (a) the $\delta = 0.06$ branch of the nonzero unstable steady-state solutions shifts to lower frequencies and lower amplitudes until it becomes tangent to the $\sigma -$ axis, (b) then the curve splits into two distinct branches, one stable and the other one unstable as for $\delta = 0.1$, (c) the gap between the two distinct branches, as $\delta = 0.1$ increases to $\delta = 0.2$, increases as well (opposite to the damping influence), (d) the branches show an increase in the softening effect, and (e) both branches continue to shift to lower frequencies. The gap between the two branches (between *B* and *C*) consists of unstable solutions; therefore, the gap increase results into a wider range of frequencies for which pull-in phenomenon occurs regardless the initial amplitude. As $\delta$ increases, the interval $(\sigma_A, \sigma_C)$ of resonant frequencies, when the resonator operates at nonzero steady-state amplitudes, broadens. In conclusion, an increase in the excitation force (voltage) broadens the range of frequencies for which the resonator becomes unstable, broadens the range of frequencies for which nonzero resonant amplitudes occur, and lowers the frequency at which resonance phenomena occur. For example, for $\sigma = -0.012$, the resonant steady-state amplitudes $U_{\max}$ are 0.6 and 0.0, for the values of $\delta = 0.1$ and $\delta = 0.2$, respectively. Hence, larger amplitudes occur at smaller excitation parameter values. Figure 5(*b*) shows no significant influence of $\delta$ on the phase–frequency response. There is a good agreement between Figs. 5(*a*) and 5(*c*) which shows the five terms ROM time response for $\sigma = -0.012$, and $\delta = 0.1$ and $\delta = 0.2$. Both models predict a reduction in amplitude with the increase in voltage. Just recently two papers regarding frequency response of electrostatically actuated MEMS cantilever resonators [45] and single wall carbon nanotube (CNT) [46], "using AUTO 07P software package for continuation and bifurcation problems is then used to numerically solve the system of equations," [45], have been reported in the literature.

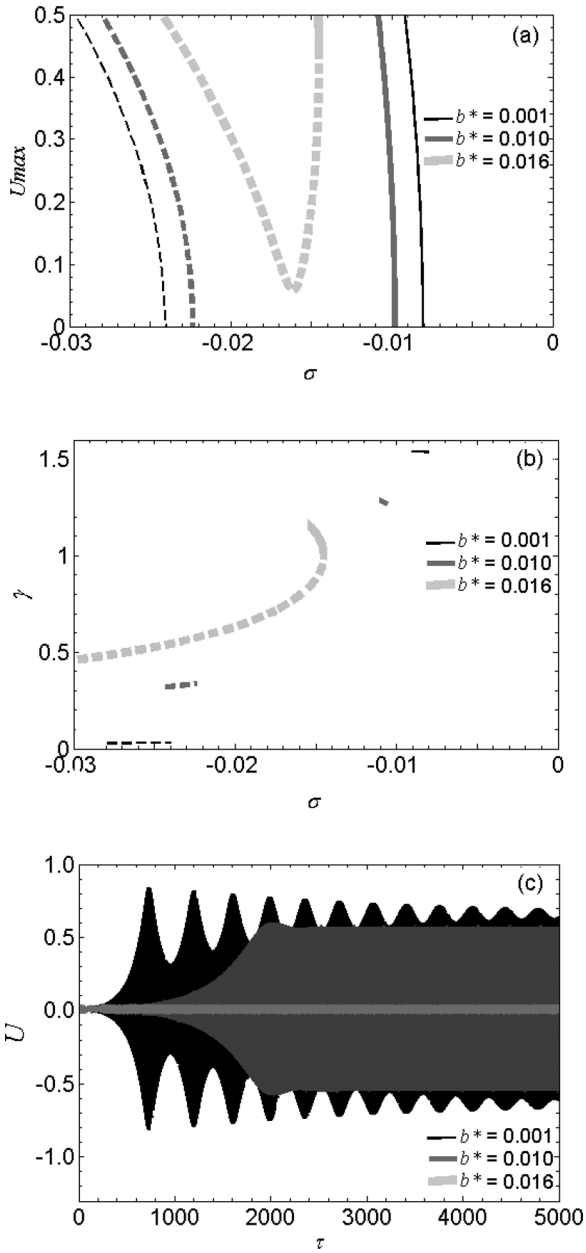


**Fig. 4 Influence of the dimensionless damping parameter $b^*$ on the frequency response. The parameters used are $\alpha = 0$, $\delta = 0.1$, and $f = 0.26$. (*a*) Amplitude–frequency response using MMS, (*b*) Phase–frequency response using MMS, and (*c*) time response using ROM for $\sigma = -0.013$ and initial amplitude $U_0 = 0$.**

Figure 6 shows the influence of the fringe effect parameter *f* on the system. As the fringe parameter increases, the stable and unstable branches are shifted to lower frequencies and the unstable region between branches (between points *B* and *C*) widens (Fig. 6(*a*)). Since the value of the fringe effect parameter depends on the gap to width ratio, Eq. (4), the fringing effect is more important for narrow beam resonators. The fringe effect enhances the electrostatic force widening the unstable region between branches. Fringe effect does not have a significant influence on the phase response (Fig. 6(*b*)). Figure 6(*c*) shows the five term

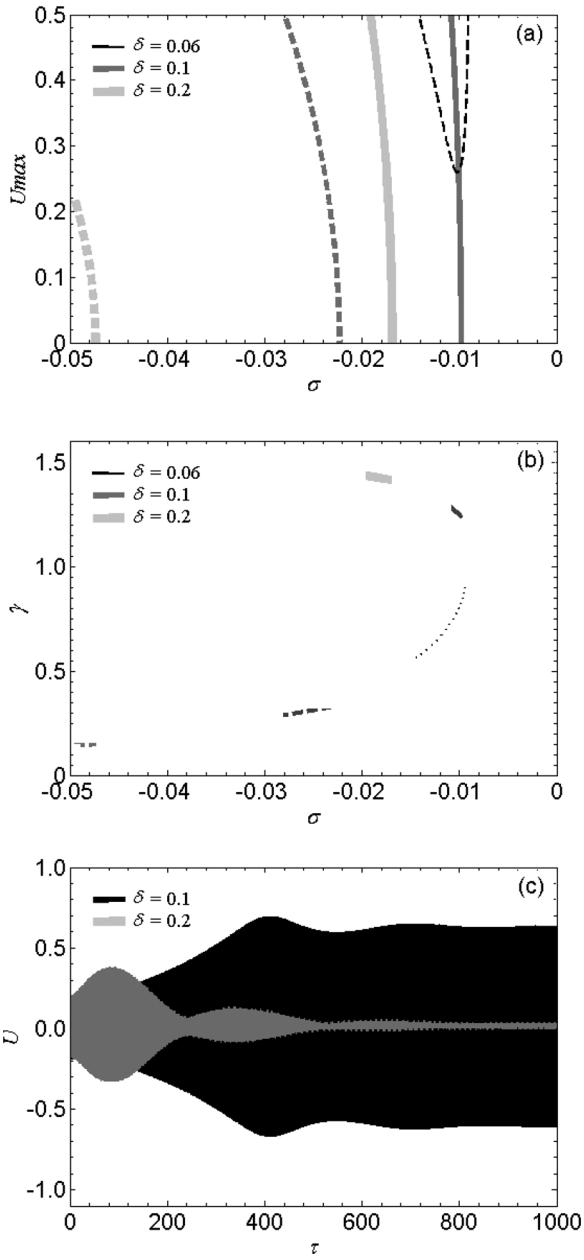


**Fig. 5 Influence of the dimensionless excitation parameter $\delta$ on the frequency response. The parameters used are $\alpha = 0$, $f = 0.26$, and $b^* = 0.01$. (*a*) Amplitude–frequency response using MMS, (*b*) phase–frequency response using MMS, and (*c*) time response using ROM for $\sigma = -0.015$ and initial amplitude $U_0 = 0.2$; as the excitation increases, the steady-state amplitude increases.**

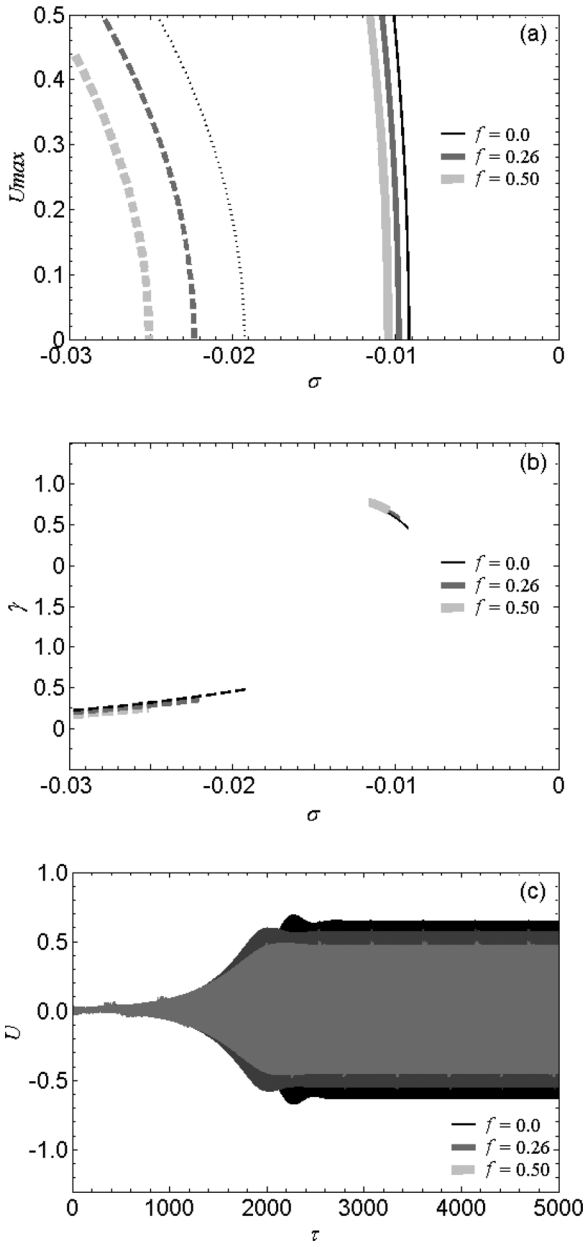


**Fig. 6 Influence of the fringe correction *f* on the frequency response. The parameters used are $\alpha = 0$, $\delta = 0.1$, and $b^* = 0.01$. (*a*) Amplitude–frequency response using MMS, (*b*) phase–amplitude response using MMS, and (*c*) time response using ROM for $\sigma = -0.013$ and initial tip displacement is $U_0 = 0$; as the fringe correction parameter increases, the steady-state amplitude increases**

ROM time response and a good agreement with Fig. 6(*a*). Fringe effect included shows a smaller value than if neglected. Therefore, neglecting the fringe effect in estimates the contribution of the electrostatic force for narrow beam elements.

This paper falls in the category of analytical investigation and numerical simulations MEMS [1,9,11,14,18,24–27,38–41]. The results of this work are in good agreement with experimental data reported in the literature [42,43]. Both Refs. [42,43] reported a softening effect and Hopf bifurcations for MEMS cantilever parametric resonance.

As application, the proposed MEMS resonator can be used as microbalance, i.e., mass sensing device. As the mass of the MEMS resonator increases due to mass deposition, the frequency of the subcritical Hopf bifurcation, point *B* in Fig. 3(*a*), is shifted to lower values. This shift in frequency predicts the amount of mass added to the MEMS [43,44]. Similarly, bifurcation point *C* and pull-in instability point *A* are shifted to lower frequencies due to mass deposition. Just recently two papers regarding frequency response of electrostatically actuated MEMS cantilever resonators [45] and single wall CNT [46], "using AUTO 07P software package for continuation and bifurcation problems is then used to numerically solve the system of equations," [45], have been reported in the literature.

The limitations of this investigation are: (1) the use of Palmer formula for fringe effects which is not accurate for much narrower electrostatically actuated beams [37]. However, Caruntu et al. [25,26] showed the validity of Palmer formula for the investigated microbeam. (2) This work does not include experimental validation, which makes the object of future investigation.

## Acknowledgment

This material is based on research sponsored by Air Force Research Laboratory under Agreement No. FA8650-07-2-5061. This work was funded by the U.S. Department of Defense (DOD), the Air Force Research Laboratory (AFRL).

## References

[1] Tetin, S., Caillar, B., Menil, H. D., Lucat, C., Pellet, C., and Dufour, I., 2010, "Modeling and Performance of Uncoated Microcantilever-Based Chemical Sensors," Sens. Actuators, B, **143**(2), pp. 555–560.
[2] Ricciardi, C., Canavese, G., Castagna, R., Ferrante, I., Ricci, A., Marasso, S. L., Napione, L., and Bussolino, F., 2010, "Integration of Microfluidic and Cantilever Technology for Biosensing Application in Liquid Environment," Biosens. Bioelectron., **26**(4), pp. 1565–1570.
[3] Bianco, S., Cocuzza, M., Ferrero, S., Giuri, E., Piacenza, G., Pirri, C. F., Ricci, A., and Scaltrito, L., 2006, "Silicon Resonant Mirocatilevers for Absolute Pressure Measurement," J. Vac. Sci. B, **24**(4), pp. 1803–1809.
[4] Joglekar, M. M., and Pawaskar, D. N., 2011, "Estimation of Oscillation Period/Switching Time for Electrostatically Actuated Microbeam Type Switches," Int. J. Mech. Sci., **53**(2), pp. 116–125.
[5] Harb, A., 2010, "Energy Harvesting: State-of-the-Art," Renewable Energy, **36**(10), pp. 2641–2654.
[6] Lamoreaux, S. K., 2005, "The Casimir Force: Background, Experiments, and Applications," Rep. Prog. Phys., **68**(1), pp. 201–236.
[7] Okada, H., Itoh, T., and Suga, T., 2008, "Wafer Level Sealing Characterization Method Using Si Micro Cantilevers," Sens. Actuators, A, **147**(2), pp. 359–364.
[8] Blom, F. R., Bouwstra, S., Elwenspoek, M., and Fluitman, J. H. J., 1992, "Dependence of the Quality Factor Of Micromachined Silicon Beam Resonators on Pressure and Geometry," J. Vac. Sci. Technol. B, **10**(1), pp. 19–26.
[9] Jazar, R. N., Mahinfalah, M., Mahmoudian, N., and Rastgaar, M. A., 2009, "Effects of Nonlinearities on the Steady State Dynamic Behavior of Electric Actuated Microcantilever-Based Resonators," J. Vib. Control, **15**(9), pp. 1283–1306.
[10] Palmer, H. B., 1937, "Capacitance of a Parallel-Plate Capacitor by the Schwartz–Christoffel Transformation," Trans. Am. Inst. Electron. Eng., **56**(3), pp. 363–366.
[11] Caruntu, D. I., and Knecht, M. W., 2011, "On Nonlinear Response Near-Half Natural Frequency of Electrostatically Actuated Microresonators," Int. J. Struct. Stability Dyn., **11**(4), pp. 641–672.
[12] Krylov, S., 2008, "Parametric Excitation and Stabilization of Electrostatically Actuated Microstructures," Int. J. Multiscale Comput. Eng., **6**(6), pp. 563–584.
[13] Krylov, S., Harari, I., and Cohen, Y., 2005, "Stabilization of Electrostatically Actuated Microstructures Using Parametric Excitation," J. Micromech. Microeng., **15**(6), pp. 1188–1204.
[14] Nayfeh, A. H., Younis, M. I., and Abdel-Rahman, E. M., 2007, "Dynamic Pull-In Phenomenon in MEMS Resonantors," Nonlinear Dyn., **48**(1–2), pp. 153–163.
[15] Sader, J. E., 1998, "Frequency Response of Cantilever Beams Immersed in Viscous Fluids With Applications to Atomic Force Microscope," J. Appl. Phys., **84**(1), pp. 64–76.
[16] Green, C. P., and Sader, J. E., 2005, "Small Amplitude Oscillations of a Thin Beam Immersed in a Viscous Fluid Near a Solid Surface," Phys. Fluids, **17**(7), pp. 1–12.
[17] Van Eysden, C. A., and Sader, J. E., 2006, "Small Amplitude Oscillation of a Flexible Thin Blade in a Viscous Fluid: Exact Analytical Solution," Phys. Fluids, **18**(12), p. 123102.
[18] Van Eysden, C. A., and Sader, J. E., 2007, "Frequency Response of Cantilever Beams Immersed in Viscous Fluids With Application to the Atomic Force Microscope: Arbitrary Mode Order," J. Appl. Phys., **101**(4), p. 044908.
[19] Brumley, D. R., Willcox, M., and Sader, J. E., 2010, "Oscillation of Cylinders of Rectangular Cross Section Immersed in Fluid," Phys. Fluids, **22**(5), pp. 1–15.
[20] Sader, J. E., Burg, T. P., Lee, J., and Manalis, S. R., 2011, "Energy Dissipation in Microfluidic Beam Resonators: Effect of Poisson's Ratio," Phys. Rev. E, **84**(2), p. 026304.
[21] Sader, J. E., Hughes, B. D., Sanelli, J. A., and Bieske, E. J., 2012, "Effect of Multiplicative Noise on Least-Squares Parameter Estimation With Application to the Atomic Force Microscope," Rev. Sci. Instrum., **83**(5), p. 055106.
[22] Prakash, G., Raman, A., Rhoads, J., and Reifenberger, R. G., 2012, "Parametric Noise Squeezing and Parametric Resonance of Microcantilevers in Air and Liquid Environments," Rev. Sci. Instrum., **83**(6), p. 065109.
[23] Turner, K., Miller, S., Hartwell, P., MacDonald, N., Strogatz, S., and Adams, S., 1998, "Five Parametric Resonances in a Microelectromechanical System," Nature, **396**(1), pp. 149–152.
[24] Nayfeh, A. H., Younis, M. I., and Abdel-Rahman, E. M., 2005, "Reduced-Order Models for MEMS Applications," Nonlinear Dyn., **41**(1–3), pp. 211–236.
[25] Caruntu, D. I., Martinez, I., and Taylor, K. N., 2013, "Voltage-Amplitude Response of Alternating Current Near Half Natural Frequency Electrostatically Actuated MEMS Resonators," Mech. Res. Commun., **52**(1), pp. 25–31.
[26] Caruntu, D. I., Martinez, I., and Knecht, M. W., 2013, "ROM Analysis of Frequency Response of AC Near Half Natural Frequency Electrostatically Actuated MEMS Cantilevers," ASME J. Comput. Nonlinear Dyn., **8**(3), p. 031011.
[27] Younis, M. I., and Nayfeh, A. H., 2003, "A Study of the Nonlinear Response of a Resonant Microbeam to an Electric Actuation," Nonlinear Dyn., **31**(1), pp. 91–117.
[28] Timoshenko, S., Young, D. H., and Weaver, Jr., W., 1974, *Vibration Problems in Engineering*, 4th ed., John Wiley & Sons, New York.
[29] Caruntu, D. I., 2009, "Dynamic Modal Characteristics of Transverse Vibrations of Cantilevers of Parabolic Thickness," Mech. Res. Commun., **33**(3), pp. 391–404.
[30] Caruntu, D. I., 2013, "Factorization of Self-Adjoint Ordinary Differential Equations," J. Appl. Math. Comput., **219**(14), pp. 7622–7631.
[31] Caruntu, D. I., 2013, "Eigenvalue Singular Problem of Factorized Fourth-Order Self-Adjoint Differential Equations," J. Appl. Math. Comput., **224**(1), pp. 603–610.
[32] Alsaleem, F. M., Younis, M. I., and Ouakad, H. M., 2009, "On the Nonlinear Resonances and Dynamic Pull-In of Electrostatically Actuated Resonators," J. Micromech. Microeng., **19**(4), pp. 1–14.
[33] Younis, M. I., Abdel-Rahman, E. M., and Nayfeh, A., 2003, "A Reduced-Order Model for Electrically Actuated Microbeam-Based MEMS," J. Microelectromech. Syst., **12**(5), pp. 672–680.
[34] Strogatz, S. H., 1994, *Nonlinear Dynamics and Chaos*, Perseus Books Publishing, LLC, Cambridge, MA.
[35] Ramezani, A., Alasty, A., and Akbari, J., 2008, "Analytical Investigation and Numerical Verification of Casimir Effect on Electrostatic Nano-Cantilevers," Microsyst. Technol., **14**(2), pp. 145–157.
[36] Zhu, J., Ru, C. Q., and Mioduchowski, A., 2007, "High-Order Subharmonic Parametric Resonance of Nonlinearly Coupled Micromechanical Oscillators," Eur. Phys. J. B, **58**(4), pp. 411–421.
[37] Nayfeh, A. H., 2004, *Nonlinear Oscillations*, Wiley-VCH Verlag GMBH & Co, KGaA, Weinheim.
[38] Batra, R. C., Porfiri, M., and Spinello, D., 2006, "Electromechanical Model of Electrically Actuated Narrow Beams," J. Microelectromech. Syst., **15**(5), pp. 1175–1189.
[39] Askari, A. R., and Tahani, M., 2014, "An Alternative Reduced Order Model for Electrically Actuated Micro-Beams Under Mechanical Shock," Mech. Res. Commun., **57**(1), pp. 34–39.
[40] Gutschmidt, S., and Gottlieb, O., 2012, "Nonlinear Dynamic Behavior of a Microbeam Array Subject to Parametric Actuation at Low, Medium and Large DC-Voltages," Nonlinear Dyn., **67**(1), pp. 1–36.
[41] Ouakad, H. M., and Younis, M. I., 2010, "The Dynamic Behavior of MEMS Arch Resonators Actuated Electrically," Int. J. Non-Linear Mech., **45**(7), pp.704–713.
[42] Younis, M. I., and Alsaleem, F., 2009, "Exploration of New Concepts for Mass Detection in Electrostatically-Actuated Structures Based on Nonlinear Phenomena," ASME J. Comput. Nonlinear Dyn., **4**(2), p. 021010.
[43] Napoli, M., Baskaran, R., Turner, K., and Bamieh, B., 2003, "Understanding Mechanical Domain Parametric Resonance in Microcantilevers," Proceedings of IEEE MicroElectro Mechanical Systems (MEMS), Kyoto, Japan, Jan. 19–23, pp. 169–172.
[44] Caruntu, D. I., and Knecht, M., 2010, "On Electrostatically Actuated Microsenors," Proc. SPIE, **7647**(1), p. 764713.
[45] Caruntu, D. I., and Martinez, I., 2014, "Reduced Order Model of Parametric Resonance of Electrostatically Actuated MEMS Cantilever Resonators," Int. J. Non-Linear Mech., **66**(1), pp. 28–32.
[46] Caruntu, D. I., and Luo, L., 2014, "Frequency Response of Primary Resonance of Electrostatically Actuated CNT Cantilevers," Nonlinear Dyn., **78**(1), pp. 1827–1837.